



## RESEARCH PAPER

## OPEN ACCESS

## Biosynthesis of TiO<sub>2</sub> nanoparticles using red seaweed: Detailed characterization

Swapnil B. Patil, D. B. Nakade\*

*Department of Microbiology, Rajaram College, Kolhapur (Maharashtra), India*

**Key words:** TiO<sub>2</sub>, Nanoparticles, Red seaweed, Biosynthesis

<http://dx.doi.org/10.12692/ijb/26.3.36-45>

Article published on March 06, 2025

### Abstract

This research presents the green synthesis of titanium dioxide (TiO<sub>2</sub>) nanoparticles (NPs) using red seaweed extract and their comprehensive characterization through various analytical techniques. The synthesis process yielded spherical and crystalline TiO<sub>2</sub> NPs with sizes ranging from 93.20 to 110.5 nm. Characterization was performed using SEM, TEM, FTIR, XRD, DLS, and AFM analyses. SEM and TEM revealed highly crystalline structures with well-defined lattice fringes, confirming their suitability for photocatalytic applications. FTIR analysis indicated the presence of organic residues and the successful formation of TiO<sub>2</sub>. XRD analysis identified prominent peaks corresponding to anatase and rutile phases, with minor indications of brookite phase or impurities. DLS measurements showed a Z-average diameter of 114 nm with a moderately broad size distribution (PDI of 0.34). AFM analysis highlighted the moderately rough surface and high surface area, enhancing photocatalytic efficiency. This study underscores the potential of red seaweed extract-mediated synthesis as a green, sustainable method for producing TiO<sub>2</sub> NPs with promising photocatalytic properties, suggesting further optimization for enhanced applications in environmental remediation and antimicrobial treatments.

\* **Corresponding Author:** D. B. Nakade ✉ [nakadedhanraj@gmail.com](mailto:nakadedhanraj@gmail.com)

## Introduction

Innovation and scientific discoveries are witnessing a significant expansion in the area of nanomaterials. Particles in the 1 to 100 nm size range are classified as organic or inorganic nanomaterials (Ahmad *et al.*, 2020). Different synthesis approaches, such as chemical, physical, and green synthesis procedures, have been employed in the synthesis of nanoparticles. As a result of their continued evolution, these technologies continue to face issues with aggregation and stability, and control over crystal growth, size, shape, and distribution. Additionally, as more applications rise to prominence, the separation of the generated nanoparticles becomes crucial (Makarov *et al.*, 2014). An improvement over chemical and physical methods is provided by the biosynthetic approach to green technology, which uses bacteria, actinomycetes, yeasts, fungus, algae, and plant extract (Aravind *et al.*, 2021). According to Makarov *et al.* (2014), it can also be effectively scaled up for large-scale production, reduce the need for harmful chemicals, be economical, environmentally benign, and more energy-efficient without requiring high pressure or temperature (Keat *et al.*, 2015).

Even though chemical and physical techniques are widely utilized to produce nanoparticles, they necessitate the employment of hazardous and reactive reducing agents, including hydrazine hydrate, N, N-dimethyl formamide (DMF), sodium borohydride (NaBH<sub>4</sub>), and Tollen's reagent (Tran *et al.*, 2018). According to Saif *et al.* (2016), this will have unfavourable negative effects on the ecosystem and the plant and animal life it supports.

TiO<sub>2</sub> NPs (Titanium dioxide nanoparticles) are considered one of the most significant NPs due to their photo-catalytic activity, chemical and thermal stability, and affordability (Muniandy *et al.*, 2017; Ahn *et al.*, 2022). The biosynthesis of nanoparticles has garnered considerable attention in recent years due to the growing need for nontoxic chemicals, antiviral, antibacterial, diagnostic, anticancer, specific drug delivery, environmentally friendly solvents, and renewable materials (Subhapiya and Gomathipriya,

2018). Natural products from medicinal plants, including *Curcuma longa*, *Vigna unguiculata*, *Eclipta prostrata*, *Ageratina altissima* L, *Calotropis gigantean*, *Psidium guajava*, *Aloe barbadensis* Miller, *Vitex negundo*, and *Moringa oleifera*, have been used by several investigators to produce TiO<sub>2</sub> nanoparticles (Subhapiya and Gomathipriya, 2018). Plants are a great source of nanoparticles, and most products manufactured from them are safe. TiO<sub>2</sub> NPs' biocompatible and non-toxic properties make them useful for pharmaceutical and biomedical sciences, including bone tissue engineering. As a result, it may be possible to enhance current methods for producing titanium nanoparticles.

Algae nanoparticles are secure, environmentally benign, and relatively stable in various applications. Additionally, algal cells are abundantly utilized as biomaterials for food (Ahmad *et al.*, 2024), feed (Ashour *et al.*, 2021a), fertilizers (Ashour *et al.*, 2021b), bioenergy (Alprol *et al.*, 2021), and wastewater treatment (Khalaf, 2008). Seaweeds have high metal-binding capacities because their cell wall surfaces contain proteins, polysaccharides, and lipids with a variety of functional groups (Mansour *et al.*, 2022). In the current work, red seaweed (*Ceramium diaphanum*) aqueous extract was used to biosynthesize TiO<sub>2</sub> NPs, which were then examined using FTIR, XRD, AFM, SEM, and TEM. Consequently, this approach may be suitable for the development of a biological method for the bulk production of nanoparticles.

## Materials and methods

### Plant material

The specimen of *Ceramium diaphanum*, a type of red seaweed, was obtained from the Kunkeshwar coastline in Maharashtra, India. The seaweed was identified and authenticated by the Department of Botany at Sadguru Gadge Maharaj College in Karad, Maharashtra. The collected sample was rinsed with seawater to eliminate epiphytes and sand particles. The sample was then placed in a polythene bag and transported to the laboratory. The specimen was cleansed using clean water and

then air-dried in a shaded area for duration of one week.

The sun-dried seaweed was pulverized into a fine powder using an electric grinder and then used for characterization.

#### *TiO<sub>2</sub> NP synthesis*

The preparation of the extract involved combining 50 g of algae with 100 ml of distilled water and subjecting the mixture to boiling on a hotplate for duration of 30 minutes.

Subsequently, the solution containing water was subjected to filtration. 50 ml of titanium tetra isopropoxide (TTIP) was taken out and placed in a 100 ml beaker. Then, 20 ml of extract was slowly added to the TTIP solution, one drop at a time. The solution was agitated for 3 hours at ambient temperature. The solution transforms from a pristine white hue to a slightly yellowish-grey shade. The confirmation of TiO<sub>2</sub> NPs production was indicated by a change in color. At last, the solution underwent filtration and was subjected to a drying process at a temperature of 110°C for duration of 5 hours. The dehydrated samples were subjected to calcination in a Muffle furnace at a temperature of 500 °C for duration of 2 hours. The chemicals used in this study were obtained from HIMEDIA™, a supplier based in Maharashtra, India, and were of analytical reagent (AR) grade.

#### *Characterization of TiO<sub>2</sub> NPs*

To visualize the surface texture, particle size, and elemental composition of nanoparticles, SEM (Scanning electron microscopy) analysis was performed. SEM–EDX evaluation was performed jointly utilizing a JSM-IT200 SEM from JEOL USA. A Fourier-infrared spectrometer (FTIR) was used to determine the functional groups on the surface of TiO<sub>2</sub> NPs (Bruker Alpha-II). The Sigma-Aldrich IR Spectrum Table & Chart (<https://www.sigmaaldrich.com/IN/en/technical-documents/technical-article/analytical-chemistry/photometry-and-reflectometry/ir-spectrum-table>) was utilized to identify functional groups. An X-ray diffraction investigation (XRD) was conducted

utilizing a D2 Phaser model supplied by Bruker Ltd. in Germany. Utilizing a JEOL Electron Micro analyzer, electronic spectroscopic imaging, and the TEM (Transmission Electron Microscopy) examination was carried out. The size and distribution of molecules and particles were measured by applying the HORIBA SZ-100 Ver. 2.40 DLS (dynamic light scattering) analysis. AFM (Atomic Force Microscopy) examination was performed utilizing the Hitachi High Tech to analyze the topography of surfaces.

## **Results and discussion**

### *Characterization*

Fig. 1 and 2 show the SEM and TEM images of TiO<sub>2</sub> NPs. The clustered spherical particles represent TiO<sub>2</sub> nanoparticles. Their sizes varied (93.20–110.5 nm), but they appeared uniform in shape (Haider *et al.*, 2017). Agglomeration of TiO<sub>2</sub> nanoparticles is evident in the image (Dubey *et al.*, 2019). Fig. 2A image revealed the crystalline nature of the TiO<sub>2</sub> NPs providing clear evidence of a highly ordered crystalline structure (Bekele *et al.*, 2020). Fig. 2B, captured at a slightly lower magnification, offered additional insights into the nanoparticle structure. Both figures clearly showed the presence of lattice fringes and distinct grain boundaries. These structural features were highly beneficial for photocatalytic applications, as grain boundaries and crystalline interfaces provide trapping sites for electrons and holes required for better photocatalysis (Jelovica Badovinac *et al.*, 2020). The well-resolved lattice planes and grain structure in both Fig. 2A and Fig. 2B underscored these TiO<sub>2</sub> NPs nanoparticles show well-defined morphology along with suitable characteristics (Farrugia *et al.*, 2021). Fig. 2C showed the irregular agglomeration of TiO<sub>2</sub> NPs, and Fig. 2D showed the SAED (Selected Area Electron Diffraction) patterns demonstrating the crystalline nature due to distinct diffraction rings indicating that the TiO<sub>2</sub> NPs are crystalline. Sharp rings suggested a high degree of crystallinity (Huq, 2020), which is beneficial for photocatalytic applications as it can enhance electron-hole pair separation and reduce recombination rates.

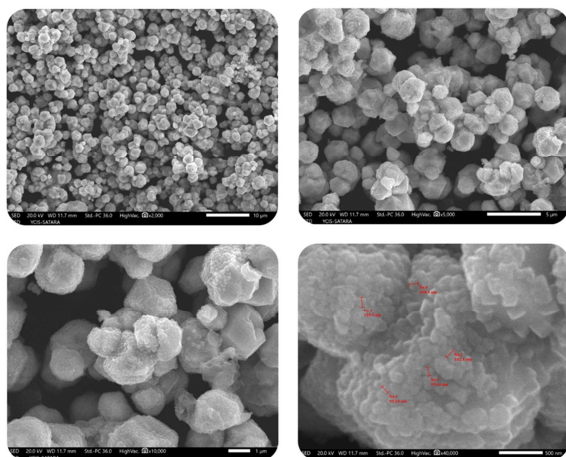


**Fig. 1.** SEM analysis of TiO<sub>2</sub> NPs

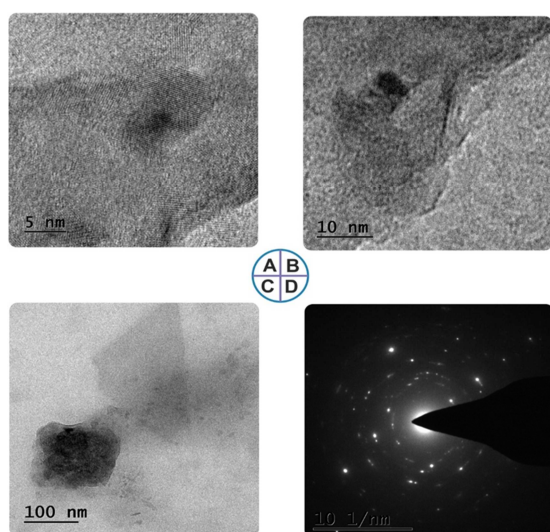


**Fig. 2.** TEM analysis of TiO<sub>2</sub> NPs

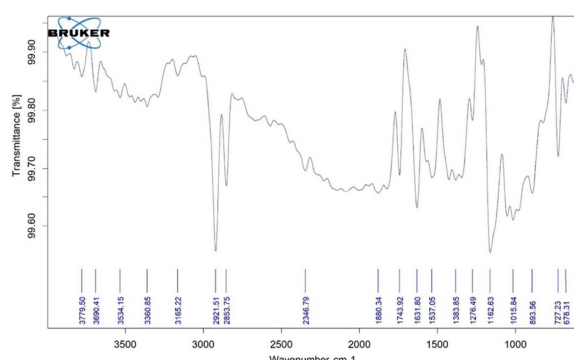


**Fig. 3.** FTIR analysis of TiO<sub>2</sub> NPs

Fig. 3 displays the FTIR spectrum for the synthesized TiO<sub>2</sub> NPs. The peaks at 3779.50 cm<sup>-1</sup>, 3534.15 cm<sup>-1</sup>, 3360.85 cm<sup>-1</sup>, and 3690.41 cm<sup>-1</sup> corresponded to O-H stretching vibrations. The TiO<sub>2</sub> nanoparticles showed the existence of hydroxyl groups, possibly

from TiO<sub>2</sub> surface groups (León *et al.*, 2017). A peak at 3165.22 cm<sup>-1</sup> reflected the stretching vibration of C-H bonds. It suggested that organic contaminants were present throughout the nanoparticle production process. The peaks at 2921.51 cm<sup>-1</sup> and 2853.75 cm<sup>-1</sup> showed aliphatic C-H stretching vibrations, indicating organic residues or surface-bound organic compounds. The peaks at 1880.34 cm<sup>-1</sup> and 1743.92 cm<sup>-1</sup> corresponded to carbonyl stretching vibrations (Matouke, 2019). The peak at 1631.80 cm<sup>-1</sup> and 1537.05 cm<sup>-1</sup> was caused by N-H bending vibrations. A peak at 1383.85 cm<sup>-1</sup> was connected with the bending vibration of CH<sub>3</sub> groups, which indicated organic material (Nguyen and Bark, 2020). The peak at 1276.49 cm<sup>-1</sup> corresponds to C-O stretching vibrations, indicating the occurrence of organic esters or ethers. The peak at 1162.63 cm<sup>-1</sup> indicated the existence of C-O-C stretching vibrations. A peak at 1015.84 cm<sup>-1</sup> demonstrated Si-O stretching vibrations, which could imply silica impurity or surface coating. Si-O-Si bending vibrations had a distinctive peak at 893.56 cm<sup>-1</sup>, supporting silica's presence. The peaks at 727.23 cm<sup>-1</sup> and 678.31 cm<sup>-1</sup> correspond to Ti-O-Ti stretching vibrations, indicating the presence of TiO<sub>2</sub> nanoparticles (Mugundan *et al.*, 2015).

TiO<sub>2</sub> nanoparticles' FTIR spectrum reveals distinct peaks for O-H, C-H, C=O, and Ti-O-Ti vibration. The existence of peaks linked with organic molecules shows that organic leftovers were used in the production process. Peaks corresponding to hydroxyl groups and water molecules indicate moisture adsorption, which is frequent for nanoparticles due to their large surface area. Silica-related peaks could indicate contamination.

The powder XRD of TiO<sub>2</sub> revealed its crystalline nature, with diffraction peaks corresponding to the rutile and anatase phases of TiO<sub>2</sub> (Fig. 4). These patterns showed that both forms of TiO<sub>2</sub> NPs were crystalline with well-defined peaks indicating a high degree of crystallinity (Sharma *et al.*, 2014). The peaks at 35°, 54°, and 63° were strong indicators of the anatase phase of TiO<sub>2</sub>. The anatase phase is the

most common and stable form of  $\text{TiO}_2$  nanoparticles (Manikandan *et al.*, 2017). A peak at  $26^\circ$  corresponded to the (110) plane of the rutile phase  $\text{TiO}_2$ . The peak at  $43^\circ$  corresponds to the (210) plane of rutile  $\text{TiO}_2$ . The peak at  $57^\circ$  corresponds to the (220) plane of rutile phase  $\text{TiO}_2$ . A peak at  $74^\circ$  corresponds to the (112) plane of the rutile phase  $\text{TiO}_2$  (Nguyen and Bark, 2020).  $\text{TiO}_2$  rutile particles appear to be more elongated silhouettes, possibly due to the interface nucleation process and growth during the phase transition (Santos-Aguilar *et al.*, 2023). A peak at  $30^\circ$  this peak is connected with the (121) plane of brookite phase  $\text{TiO}_2$  or might suggest the existence of impurities or other chemicals added during the synthesis with red seaweed extract. The XRD spectrum of  $\text{TiO}_2$  nanoparticles produced with red seaweed extract revealed distinct peaks related to the rutile phase of  $\text{TiO}_2$ . The prominent peaks at  $26^\circ$ ,  $35^\circ$ ,  $54^\circ$ ,  $57^\circ$ , and  $63^\circ$   $2\theta$  confirmed the presence of the anatase and rutile phase in the produced nanoparticles. The peak at  $30^\circ$   $2\theta$  may indicate the presence of brookite or contaminants from the synthesis process.

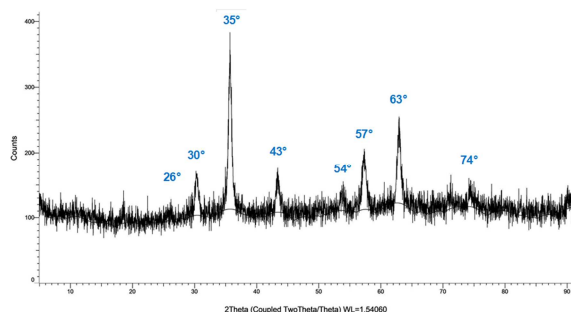


**Fig. 4.** XRD analysis of  $\text{TiO}_2$  NPs

Fig. 5 represents the DLS measurement for the  $\text{TiO}_2$  NPs. Z-average (Hydrodynamic diameter), is the average diameter of the particles in suspension, considering their size and shape. A higher Z-average value indicates larger particles (Panda *et al.*, 2018). In this case, the Z-average diameter of the  $\text{TiO}_2$  nanoparticles is 114 nm, which is relatively large for nanoparticles (Santos-Aguilar *et al.*, 2023). Polydispersity Index (PI) is a measure of the distribution of particle sizes in a sample. A PDI value closer to 0 indicates a more uniform size distribution,

while a higher value indicates a broader distribution (Adhikary *et al.*, 2023).

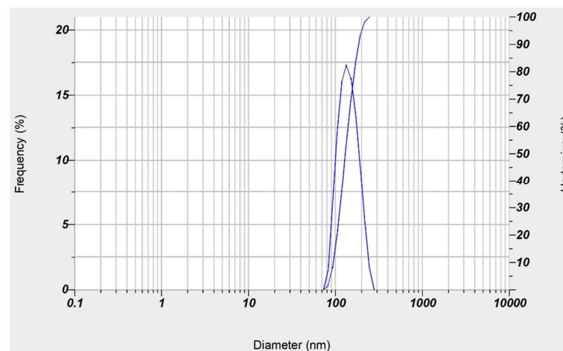


**Fig. 5.** DLS analysis of  $\text{TiO}_2$  NPs

In this case, the PI value of 0.34 suggested a moderately broad size distribution of the  $\text{TiO}_2$  nanoparticles. A PDI value less than 0.1 is considered monodisperse, while a value greater than 0.5 is considered polydisperse (Younis *et al.*, 2023). In summary, the DLS analysis indicates that your  $\text{TiO}_2$  nanoparticles are relatively large (114 nm) and have a moderately broad size distribution.

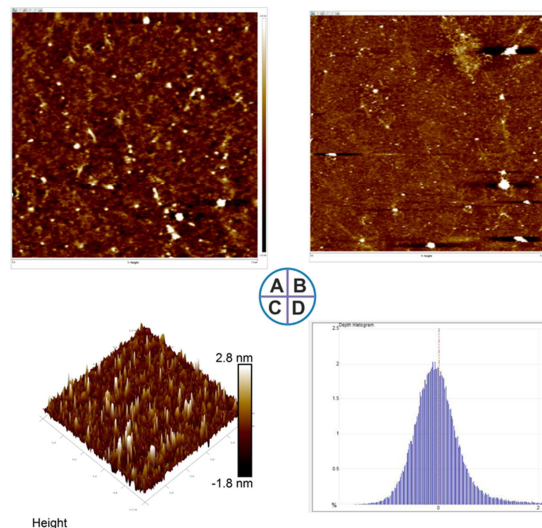


**Fig. 6.** AFM analysis of  $\text{TiO}_2$  NPs

Figs 6A and 6B display the surface morphology of the  $\text{TiO}_2$  nanoparticles. Fig. 6C shows the surface roughness of the  $\text{TiO}_2$  materials, while Fig. 6D shows the depth distribution of  $\text{TiO}_2$  nanoparticles. The Atomic Force Microscopy (AFM) data offers an intricate characterization of the surface attributes of

TiO<sub>2</sub> nanoparticles. This examination concentrated on pivotal metrics, including roughness, surface area, and additional statistical properties. These metrics were essential in assessing the photocatalytic capabilities of the TiO<sub>2</sub> nanoparticles (Asakawa *et al.*, 2018). Fig. 6A at 1 μm scale showed a dense distribution of TiO<sub>2</sub> NPs with a relatively rough surface topography. Individual nanoparticles and small clusters are visible, indicating a high agglomeration with a uniform distribution of nanoparticles. The visual inspection indicated a moderately rough surface with numerous peaks and valleys. Fig. 6B at 5 μm Scale image showed less densely packed with the heterogeneous distribution of nanoparticles than Fig. 6A. Also, it is evident that there was a large height variation. The surface appeared less densely packed than Fig. 6A, showing larger features and more pronounced height variations. The surface appeared at this 5-μm scale with larger topography and deeper valleys than Fig 6A. Fig. 6A and 6B showed evidence of nanoparticle agglomeration with higher surface variation. The Skewness and Kurtosis suggested that the surface is textured; having peaks and valleys revealed that it has a higher surface (Kumar and Rao, 2012; Petrochenko *et al.*, 2015). The surface variation in the nanoscale is essential in various applications such as photocatalysis (Khan *et al.*, 2019). Fig. 6C shows the 3D topology of the TiO<sub>2</sub> nanoparticles. The height map exhibited a range from -1.8 nm to 2.8 nm, indicating the presence of nanoscale surface roughness alongside marked height variations. The presence of sharp peaks and deep valleys suggested a highly textured surface. Furthermore, the Rq and Ra parameters (Table 1) demonstrated that the surface exhibits moderate smoothness and texture characteristics, making it suitable for photocatalysis applications (Pellegrino *et al.*, 2019). Furthermore, the R-max values showed the presence of valleys and peaks, suggesting a higher surface area that is also helpful in a higher reaction rate (Amano *et al.*, 2010). Fig. 6D shows the dept histogram, which statistically represents the surface topography. The X-axis represented the height values (in nm), and the Y-axis showed the frequency of these values as a percentage

area with sharp peaks worthy of photocatalysis applications. The dept histogram also showed the peak and valley equally nearly distributed throughout the film.

**Table 1.** AFM analysis parameters of TiO<sub>2</sub> nanoparticles

Sl	Parameters	Value
1	Rq (Root Mean Square Roughness)	0.540 nm
2	Ra (Average Roughness)	0.340 nm
3	Rmax (Maximum Roughness)	103 nm
4	Skewness	3.60
5	Kurtosis	34.3

Thus, examining the TiO<sub>2</sub> nanoparticles using the data from AFM, it's clear that these particles are well-suited for use in photocatalysis. The moderate surface roughness, along with a high surface area and notable statistical features like skewness and kurtosis, indicated that these nanoparticles could significantly boost photocatalytic reactions. The presence of sharp peaks and valleys on their surface plays a pivotal role in enhancing light absorption, facilitating the generation of electron-hole pairs, and providing extensive active sites critical for heightened photocatalysis efficiency.

Titanium dioxide (TiO<sub>2</sub>), commonly known as titania, is a frequently utilized semiconductor nanoparticle with unique hydrophilic and photocatalytic properties that result in antibacterial and ultraviolet (UV) resistance (Alizadeh Sani *et al.*, 2017). These nanoparticles are widely employed in the production of polymer nanocomposites in food packaging. TiO<sub>2</sub> nanoparticles act in two ways: first, they have the potential to break biopolymeric compounds (such as polysaccharides and proteins) on their surface (Kaneko *et al.*, 2006), and second, they can change the surface characteristics of objects to a hydrophilic condition when TiO<sub>2</sub> NPs are placed on them. In Europe, TiO<sub>2</sub> (E171) has been validated and classified as a color additive in confectionaries, dairy products, and soft drinks under the 1994/36/EC Directive.

TiO<sub>2</sub> is more susceptible to oxidation when exposed to ultraviolet (UV) light with a wavelength of less than 385 nm. As a consequence, when placed under sunlight, TiO<sub>2</sub> produces active oxygen species (Alizadeh-Sani *et al.*, 2018). In addition, TiO<sub>2</sub>'s

antimicrobial ability is affected by its crystal structure, the type of artificial light, UVA light intensity, shape and size, and the formation of ROS, active radical species, hydrogen peroxide, superoxide radical, and hydroxyl radical (Bonetta *et al.*, 2013). These active species degrade the bacteria's outer membrane, specifically phospholipids, proteins, and lipopolysaccharides, causing harm to the organism.

### Conclusion

In this research, the TiO<sub>2</sub> NPs were successfully synthesized using red seaweed extract and comprehensively characterized using various analytical techniques. The SEM and TEM analyses revealed the spherical and crystalline nature of the TiO<sub>2</sub> NPs, with sizes ranging from 93.20 to 110.5 nm. The high degree of crystallinity and well-resolved lattice fringes observed in the TEM images suggested their suitability for photocatalytic applications, which require effective electron-hole pair separation. FTIR analysis identified distinct peaks corresponding to O-H, C-H, C=O, and Ti-O-Ti vibrations, indicating the presence of organic residues from the synthesis process and confirming the successful formation of TiO<sub>2</sub>. XRD analysis further confirmed the crystalline nature of the TiO<sub>2</sub> NPs, displaying prominent peaks indicative of both anatase and rutile phases. The presence of brookite phase or potential impurities was also detected, highlighting the complexity of the synthesis process using natural extracts. DLS measurements indicated a Z-average diameter of 114 nm, with a moderately broad size distribution (PDI of 0.34). AFM analysis provided detailed insights into the surface morphology, revealing a moderately rough surface with a high surface area, which is advantageous for photocatalytic applications. The surface roughness metrics and 3D topology confirmed the presence of nanoscale texture, enhancing the photocatalytic efficiency of the TiO<sub>2</sub> NPs. Overall, the red seaweed extract-mediated synthesis of TiO<sub>2</sub> NPs offers a green and sustainable approach, yielding nanoparticles with promising photocatalytic. Future work should focus on optimizing the synthesis parameters to improve the uniformity and efficacy of TiO<sub>2</sub> NPs for diverse applications in environmental remediation and antimicrobial treatments.

### References

- Adhikary K, Mandal T, Majumder J, Kumar Chowdhuri T, Singh N.** 2023. Green synthesis and characterization of TiO<sub>2</sub> nanoparticles by using ornamental grass *Cynodon dactylon* (Doob grass). *European Chemical Bulletin* **12**(5), 1713-1723.
- Ahmad S, Ahmad S, Ali S, Esa M, Khan A, Yan H.** 2024. Recent advancements and unexplored biomedical applications of green synthesized Ag and Au nanoparticles: A review. *International Journal of Nanomedicine* **19**, 3187–3215.  
<https://doi.org/10.2147/IJN.S453775>.
- Ahmad W, Jaiswal KK, Soni S.** 2020. Green synthesis of titanium dioxide (TiO<sub>2</sub>) nanoparticles by using *Mentha arvensis* leaves extract and its antimicrobial properties. *Inorganic and Nano-Metal Chemistry* **50**, 1032–1038.  
<https://doi.org/10.1080/24701556.2020.1732419>.
- Ahn EY, Shin SW, Kim K, Park Y.** 2022. Facile green synthesis of titanium dioxide nanoparticles by upcycling Mangosteen (*Garcinia mangostana*) pericarp extract. *Nanoscale Research Letters* **17**.  
<https://doi.org/10.1186/s11671-022-03678-4>.
- Alizadeh Sani M, Ehsani A, Hashemi M.** 2017. Whey protein isolate/cellulose nanofibre/TiO<sub>2</sub> nanoparticle/rosemary essential oil nanocomposite film: Its effect on microbial and sensory quality of lamb meat and growth of common foodborne pathogenic bacteria during refrigeration. *International Journal of Food Microbiology* **251**, 8–14.  
<https://doi.org/10.1016/j.ijfoodmicro.2017.03.018>.
- Alizadeh-Sani M, Khezerlou A, Ehsani A.** 2018. Fabrication and characterization of the bionanocomposite film based on whey protein biopolymer loaded with TiO<sub>2</sub> nanoparticles, cellulose nanofibers and rosemary essential oil. *Industrial Crops and Products* **124**, 300–315.  
<https://doi.org/10.1016/j.indcrop.2018.08.001>.

- Alprol AE, Heneash AMM, Ashour M, Abualnaja KM, Alhashmialameer D, Mansour AT, Sharawy ZZ, Abu-Saied MA, Abomohra AEF.** 2021. Potential applications of *Arthrospira platensis* lipid-free biomass in bioremediation of organic dye from industrial textile effluents and its influence on marine rotifer (*Brachionus plicatilis*). *Materials* **14**, 4446. <https://doi.org/10.3390/ma14164446>.
- Amano F, Nogami K, Tanaka M, Ohtani B.** 2010. Correlation between surface area and photocatalytic activity for acetaldehyde decomposition over bismuth tungstate particles with a hierarchical structure. *Langmuir* **26**, 7174–7180. <https://doi.org/10.1021/la904274c>.
- Aravind M, Amalanathan M, Mary MSM.** 2021. Synthesis of TiO<sub>2</sub> nanoparticles by chemical and green synthesis methods and their multifaceted properties. *SN Applied Sciences* **3**. <https://doi.org/10.1007/s42452-021-04281-5>.
- Asakawa H, Holmström E, Foster AS, Kamimura S, Ohno T, Fukuma T.** 2018. Direct imaging of atomic-scale surface structures of brookite TiO<sub>2</sub> nanoparticles by frequency modulation atomic force microscopy in liquid. *Journal of Physical Chemistry C* **122**, 24085–24093. <https://doi.org/10.1021/acs.jpcc.8b06262>.
- Ashour M, Alprol AE, Heneash AMM, Saleh H, Abualnaja KM, Alhashmialameer D, Mansour AT.** 2021a. Ammonia bioremediation from aquaculture wastewater effluents using *Arthrospira platensis* niof17/003: Impact of biodiesel residue and potential of ammonia-loaded biomass as rotifer feed. *Materials* **14**, 5460. <https://doi.org/10.3390/ma14185460>.
- Ashour M, Mabrouk MM, Abo-Taleb HA, Sharawy ZZ, Ayoub HF, Van Doan H, Davies SJ, El-Haroun E, Goda AMSA.** 2021b. A liquid seaweed extract (TAM®) improves aqueous rearing environment, diversity of zooplankton community, whilst enhancing growth and immune response of Nile tilapia, *Oreochromis niloticus*, challenged by *Aeromonas hydrophila*. *Aquaculture* **543**, 736915. <https://doi.org/10.1016/j.aquaculture.2021.736915>.
- Azizi-Lalabadi M, Ehsani A, Divband B, Alizadeh-Sani M.** 2019. Antimicrobial activity of titanium dioxide and zinc oxide nanoparticles supported in 4A zeolite and evaluation of morphological characteristics. *Scientific Reports* **9**, 17439. <https://doi.org/10.1038/s41598-019-54025-0>.
- Bekele ET, Gonfa BA, Zelekew OA, Belay HH, Sabir FK.** 2020. Synthesis of titanium oxide nanoparticles using root extract of *Kniphofia foliosa* as a template, characterization, and its application on drug-resistant bacteria. *Journal of Nanomaterials* 2020. <https://doi.org/10.1155/2020/2817037>.
- Bonetta S, Bonetta S, Motta F, Strini A, Carraro E.** 2013. Photocatalytic bacterial inactivation by TiO<sub>2</sub>-coated surfaces. *AMB Express* **3**, 1–8. <https://doi.org/10.1186/2191-0855-3-59>.
- Farrugia C, Di Mauro A, Lia F, Zammit E, Rizzo A, Privitera V, Impellizzeri G, Buccheri MA, Rappazzo G, Grech M, Refalo P, Abela S.** 2021. Suitability of different titanium dioxide nanotube morphologies for photocatalytic water treatment. *Nanomaterials* **11**, 1–18. <https://doi.org/10.3390/nano11030708>.

- Huq MA.** 2020. Green synthesis of silver nanoparticles using *Pseudoduganella eburnea* MAHUQ-39 and their antimicrobial mechanisms investigation against drug-resistant human pathogens. *International Journal of Molecular Sciences* **21**, 1510.  
<https://doi.org/10.3390/ijms21041510>.
- Jelovica Badovinac I, Peter R, Omerzu A, Salamon K, Šarić I, Samaržija A, Perčić M, Kavre Piltaver I, Ambrožić G, Petravić M.** 2020. Grain size effect on photocatalytic activity of TiO<sub>2</sub> thin films grown by atomic layer deposition. *Thin Solid Films* **709**.<https://doi.org/10.1016/j.tsf.2020.138215>.
- Kaneko M, Nemoto J, Ueno H, Gokan N, Ohnuki K, Horikawa M, Saito R, Shibata T.** 2006. Photoelectrochemical reaction of biomass and bio-related compounds with nanoporous TiO<sub>2</sub> film photoanode and O<sub>2</sub>-reducing cathode. *Electrochemistry Communications* **8**, 336–340.  
<https://doi.org/10.1016/j.elecom.2005.12.004>.
- Keat CL, Aziz A, Eid AM, Elmarzugi NA.** 2015. Biosynthesis of nanoparticles and silver nanoparticles. *Bioresources and Bioprocessing* **2**, 47.  
<https://doi.org/10.1186/s40643-015-0076-2>.
- Khalaf MA.** 2008. Biosorption of reactive dye from textile wastewater by non-viable biomass of *Aspergillus niger* and *Spirogyra* sp. *Bioresource Technology* **99**, 6631–6634.  
<https://doi.org/10.1016/j.biortech.2007.12.010>.
- Khan I, Saeed K, Khan I.** 2019. Nanoparticles: Properties, applications and toxicities. *Arabian Journal of Chemistry* **12**(7), 908–931.  
<https://doi.org/10.1016/j.arabjc.2017.05.011>.
- Kumar BR, Rao TS.** 2012. AFM studies on surface morphology, topography, and texture of nanostructured zinc aluminum oxide thin films. *Digest Journal of Nanomaterials and Biostructures* **7**(4), 1881–1889.
- León A, Reuquen P, Garín C, Segura R, Vargas P, Zapata P, Orihuela PA.** 2017. FTIR and Raman characterization of TiO<sub>2</sub> nanoparticles coated with polyethylene glycol as a carrier for 2-methoxyestradiol. *Applied Sciences* **7**, 49.  
<https://doi.org/10.3390/app7010049>.
- Makarov VV, Love AJ, Sinitsyna OV, Makarova SS, Yaminsky IV, Taliansky ME, Kalinina NO.** 2014. “Green” nanotechnologies: Synthesis of metal nanoparticles using plants. *Reviews* **6**(20), 14.
- Manikandan K, Ahamed AJ, Brahmanandhan GM.** 2017. Synthesis, structural and optical characterization of TiO<sub>2</sub> nanoparticles and its assessment to cytotoxicity activity. *Journal of Environmental Nanotechnology* **6**, 94–102.  
<https://doi.org/10.13074/jent.2017.09.173273>.
- Mansour AT, Alprol AE, Khedawy M, Abualnaja KM, Shalaby TA, Rayan G, Ramadan KMA, Ashour M.** 2022. Green synthesis of zinc oxide nanoparticles using red seaweed for the elimination of organic toxic dye from an aqueous solution. *Materials* **15**, 5169.  
<https://doi.org/10.3390/ma15155169>.
- Matouke MM.** 2019. FTIR study of the binary effect of titanium dioxide nanoparticles (nTiO<sub>2</sub>) and copper (Cu<sup>2+</sup>) on the biochemical constituents of liver tissues of catfish (*Clarias gariepinus*). *Toxicology Reports* **6**, 1061–1070.  
<https://doi.org/10.1016/j.toxrep.2019.10.002>.
- Mugundan S, Rajamannan B, Viruthagiri G, Shanmugam N, Gobi R, Praveen P.** 2015. Synthesis and characterization of undoped and cobalt-doped TiO<sub>2</sub> nanoparticles via sol–gel technique. *Applied Nanoscience* **5**, 449–456.  
<https://doi.org/10.1007/s13204-014-0337-y>.

- Muniandy SS, Mohd Kaus NH, Jiang ZT, Altarawneh M, Lee HL.** 2017. Green synthesis of mesoporous anatase TiO<sub>2</sub> nanoparticles and their photocatalytic activities. *RSC Advances* **7**, 48083–48094. <https://doi.org/10.1039/c7ra08187a>.
- Nguyen TMH, Bark CW.** 2020. Synthesis of cobalt-doped TiO<sub>2</sub> based on metal-organic frameworks as an effective electron transport material in perovskite solar cells. *ACS Omega* **5**, 2280–2286. <https://doi.org/10.1021/acsomega.9b03507>.
- Panda J, Singh UP, Sahu R.** 2018. Synthesis, characterization of TiO<sub>2</sub> nanoparticles for enhancement of electron transport application in DSSC with Cu-BPCA dye. *IOP Conference Series: Materials Science and Engineering* **410**, 012008. <https://doi.org/10.1088/1757-899X/410/1/012008>.
- Pellegrino F, Sordello F, Minella M, Minero C, Maurino V.** 2019. The role of surface texture on the photocatalytic H<sub>2</sub> production on TiO<sub>2</sub>. *Catalysts* **9**, 32. <https://doi.org/10.3390/catal9010032>.
- Petrochenko PE, Kumar G, Fu W, Zhang Q, Zheng J, Liang C, Goering PL, Narayan RJ.** 2015. Nanoporous aluminum oxide membranes coated with atomic layer deposition-grown titanium dioxide for biomedical applications: An *in vitro* evaluation. *Journal of Biomedical Nanotechnology* **11**, 2275–2285. <https://doi.org/10.1166/jbn.2015.2169>.
- Saif S, Tahir A, Chen Y.** 2016. Green synthesis of iron nanoparticles and their environmental applications and implications. *Nanomaterials* **6**, 209. <https://doi.org/10.3390/nano6110209>.
- Santos-Aguilar P, Bernal-Ramírez J, Vázquez-Garza E, Vélez-Escamilla LY, Lozano O, García-Rivas GDJ, Contreras-Torres FF.** 2023. Synthesis and characterization of rutile TiO<sub>2</sub> nanoparticles for the toxicological effect on the H9c2 cell line from rats. *ACS Omega* **8**, 19024–19036. <https://doi.org/10.1021/acsomega.3c01771>.
- Sharma A, Karn RK, Pandiyan SK.** 2014. Synthesis of TiO<sub>2</sub> nanoparticles by sol-gel method and their characterization. *Journal of Basic and Applied Engineering Research* **1(9)**, 1–5.
- Subhapiya S, Gomathipriya P.** 2018. Green synthesis of titanium dioxide (TiO<sub>2</sub>) nanoparticles by *Trigonella foenum-graecum* extract and its antimicrobial properties. *Microbial Pathogenesis* **116**, 215–220. <https://doi.org/10.1016/j.micpath.2018.01.027>.
- Tran QH, Nguyen VQ, Le AT.** 2018. Corrigendum: Silver nanoparticles: Synthesis, properties, toxicology, applications and perspectives (*Adv. Nat. Sci. Nanosci. Nanotechnol.* 4 033001). *Advances in Natural Sciences: Nanoscience and Nanotechnology* **9**, 049501. <https://doi.org/10.1088/2043-6254/aad12b>.
- Younis AB, Milosavljevic V, Fialova T, Smerkova K, Michalkova H, Svec P, Antal P, Kopel P, Adam V, Zurek L, Dolezelikova K.** 2023. Synthesis and characterization of TiO<sub>2</sub> nanoparticles combined with geraniol and their synergistic antibacterial activity. *BMC Microbiology* **23**, 207. <https://doi.org/10.1186/s12866-023-02955-1>.